

Elsevier required licence: © <2018>. This manuscript version is made available under the CC-BY-NC-ND 4.0 license <http://creativecommons.org/licenses/by-nc-nd/4.0/>  
The definitive publisher version is available online at

[\[https://www.sciencedirect.com/science/article/pii/S0376738817328508?via%3Dihub\]](https://www.sciencedirect.com/science/article/pii/S0376738817328508?via%3Dihub)

1 **Transport of small and neutral solutes through reverse osmosis**  
2 **membranes: Role of skin layer conformation of**  
3 **the polyamide film**

Formatted: Font color: Auto

4 Revised manuscript submitted to

5 *Journal of Membrane Science*

6 December 2017

7 Takahiro Fujioka<sup>1,\*</sup>, Brian E. O'Rourke<sup>2</sup>, Koji Michishio<sup>2</sup>, Yoshinori Kobayashi<sup>2</sup>,  
8 Nagayasu Oshima<sup>2</sup>, Hitoshi Kodamatani<sup>3</sup>, Takuji Shintani<sup>4</sup>, Long D. Nghiem<sup>5</sup>

9 <sup>1</sup>*Water and Environmental Engineering, Graduate School of Engineering,*  
10 *Nagasaki University, 1-14 Bunkyo-machi, Nagasaki 852-8521, Japan*

11 <sup>2</sup>*National Metrology Institute of Japan, National Institute of Advanced Industrial Science and*  
12 *Technology, 1-1-1 Umezono, Tsukuba, Ibaraki 305-8568, Japan*

13 <sup>3</sup>*Division of Earth and Environmental Science, Graduate School of Science and Engineering,*  
14 *Kagoshima University, 1-21-35 Korimoto, Kagoshima 890-0065, Japan*

15 <sup>4</sup>*Division of Advanced Membrane Science and Technology, Graduate School of Science,*  
16 *Technology and Innovation, Kobe University, 1-1 Rokkodai-cho, Kobe 657-8501, Japan*

17 <sup>5</sup>*Strategic Water Infrastructure Laboratory, School of Civil Mining and Environmental*  
18 *Engineering, The University of Wollongong, NSW 2522, Australia*

19 \_\_\_\_\_  
20 \* Corresponding author: Takahiro Fujioka, Email: tfujioka@nagasaki-u.ac.jp, Ph +81 095 819 2695

21 **Abstract**

22 The polyamide skin layer of reverse osmosis (RO) membranes was characterised using  
23 advanced and complementary analytical techniques to investigate the mechanisms underlying  
24 the permeation of contaminants of emerging concern in potable water reuse – *N*-  
25 nitrosodimethylamine (NDMA) and *N*-nitrosomethylethylamine (NMEA). This study used  
26 five RO membrane samples with similar membrane properties. The five RO membrane samples  
27 spanned over a large range of water permeance (0.9–5.8 L/m<sup>2</sup>hbar) as well as permeation of  
28 NDMA (9–66%) and NMEA (3–29%). Despite ~~such distinct~~these differences among the five  
29 RO membranes, characterisations of the skin layer using positron annihilation lifetime  
30 spectroscopy, atomic force microscopy and field emission scanning electron microscopy  
31 revealed almost no variation ~~difference~~ in their free-volume hole-radius (0.270–0.275 nm),  
32 effective surface area (198–212%) and thickness (30–35 nm) of the skin layer. The results  
33 suggest that there could be other RO skin layer properties, such as the interconnectivity of the  
34 protuberances within the polyamide skin layer additional to the free-volume hole-size and  
35 thickness of the skin layer, which can also govern water and solute permeation.

36 **Keywords:** free-volume hole; *N*-nitrosodimethylamine; positron annihilation lifetime  
37 spectroscopy; potable reuse; reverse osmosis.

38

Formatted: Font color: Auto

39 **1. Introduction**

40 *N*-nitrosodimethylamine (NDMA; C<sub>2</sub>H<sub>6</sub>N<sub>2</sub>O) and *N*-nitrosomethylethylamine (NMEA;  
41 C<sub>3</sub>H<sub>8</sub>N<sub>2</sub>O) are micropollutants of significant concern in potable water reuse since they are  
42 probable carcinogenic chemicals [1]. With a molecular weight of 74 g/mol, NDMA is the  
43 smallest in the *N*-nitrosamine group. NDMA and NMEA are neutral and hydrophilic  
44 compounds at environmental pH (i.e. pH 6–8). Although reverse osmosis (RO) membrane  
45 separation can achieve excellent rejection of a range of impurities in reclaimed water including  
46 salts, macro-organics, and many micropollutants, the rejection of NDMA, NMEA and several  
47 other *N*-nitrosamines is low and highly variable because of its small molecular size and lack of  
48 charge [2-5]. Thus, they are often detectable in RO permeate at concentrations higher than  
49 guideline or target values set by water authorities around the world. For example, California  
50 has established a notification level of 10 ng/L for NDMA and a public health goal of 3 ng/L  
51 [6]. Similarly, in Australia, the guideline value of NDMA in water intended for potable reuse  
52 has been also set at 10 ng/L [7]. The low and highly variable separation performance of RO  
53 with respect to NDMA rejection necessitates post treatment by advanced oxidation (UV  
54 irradiation and H<sub>2</sub>O<sub>2</sub>) [8]. Recent research [9] suggests that NDMA rejection by RO  
55 membranes varies significantly amongst the many RO membranes available on the market.  
56 Thus, further insights which lead to better membrane selection and improvement of the  
57 separation performance of RO for *N*-nitrosamine removal can directly contribute to the  
58 economic viability and public safety of potable water reuse.

Field Code Changed

Field Code Changed

Field Code Changed

Field Code Changed

Field Code Changed

Field Code Changed

59 Given the significant importance of low molecular weight micropollutants in potable reuse,  
60 numerous previous studies have been conducted to reveal the permeation mechanisms of  
61 micropollutants through RO membranes [10-13]. The significance of steric (size) interaction  
62 between solutes and the free-volume holes within the RO membrane active skin layer has been

Field Code Changed

63 clearly demonstrated from the viewpoint of solute properties. A strong correlation between  
64 molecular size (e.g. minimum molecular width or projected area) of uncharged solutes and  
65 their removals by RO has been established [14, 15]. Nevertheless, mechanisms underlying the  
66 difference in NDMA permeation among RO membranes are still poorly understood from the  
67 perspective of membrane properties. This is mainly due to analytical limitations in  
68 characterising the membrane skin layer at sub-nanometre scale resolution.

Field Code Changed

69 The free-volume holes – holes in the membrane skin layer in polymeric matrix – are thought  
70 to play an important role in water and solute transport through the RO membrane. Nevertheless,  
71 findings to date remain inconclusive. The free-volume hole size can be determined by positron  
72 annihilation lifetime spectroscopy (PALS) [16]. Previous measurements of the free-volume  
73 hole-radius of commercial RO membranes [16-18] varied considerably from 0.20 and 0.29 nm.  
74 Several previous studies [18-20] have demonstrated a strong correlation between solute  
75 permeation and free-volume hole-size. In contrast, no clear correlation between solute  
76 permeation and free-volume hole-size was reported by several other studies [17, 21, 22]. To  
77 date, there have been very few PALS studies on the characterisation of RO membranes due to  
78 the limited availability of slow positron beam based instruments.

Field Code Changed

Field Code Changed

Field Code Changed

Field Code Changed

79 The thickness of the skin layer has also been considered as an important property of an RO  
80 membrane governing water and solute transport. According to the solution-diffusion model  
81 [23-25], permeation of solutes and solution through RO membranes occurs via their penetration  
82 into the membrane material and diffusion through the RO membrane. The key role of the  
83 polymeric membrane thickness on solute permeation can also be supported by the finding that  
84 the thickness is inversely proportional to water permeance and there is a trade-off between  
85 water permeance and solute selectivity [26, 27]. This mechanism is plausible, however, it is  
86 difficult to validate for commercial RO membranes. Recent RO membranes are designed with

Field Code Changed

Field Code Changed

87 a rougher membrane surface that holds a higher surface area and a higher permeance [28-32].  
88 As a result, they commonly have a so-called “ridge-and-valley” structure and hollow interior  
89 of crumpled nodules throughout the surface of the skin layer [29]. The entire thickness of the  
90 skin layer of commercial RO membranes is about 200-300 nm as reported by previous studies  
91 using transmission electron microscopy (TEM) [33-36]. The crumpled film forming the  
92 crumpled structure of the skin layer and the flat film comprising the interface between  
93 polyamide and polysulfone layers both have a thickness as low as 20 nm [31, 37, 38].  
94 Characterisation using a field emission - scanning electron microscope (FE-SEM) [37] allows  
95 for a quantification of each polyamide film. Nevertheless, due to the complex inner structure  
96 and rough surface morphology of the RO membrane skin layer and its variation among RO  
97 membranes, it is still difficult to identify the location of the most important polyamide films  
98 and quantify their thickness for comparison among different RO membranes.

99 A systematic evaluation of several RO membranes with similar chemical ingredients can  
100 potentially yield new insights into the role of the membrane skin layer on solute permeation.  
101 This study aims to identify key structure parameters that govern NDMA transport in the RO  
102 process by characterising the skin layer properties of five RO membranes that have similar  
103 chemical composition and skin layer structure. State-of-the-art analytical techniques including  
104 PALS, FE-SEM and atomic force microscopy (AFM) were used for the characterisation of the  
105 skin layer including free-volume hole-size, thickness and surface area, respectively.

## 106 **2. Materials and methods**

### 107 **2.1. Chemicals**

108 Analytical grade NDMA and *N*-nitrosomethylethylamine (NMEA) (**Table 1**) were purchased  
109 from Ultra Scientific (Kingstown, RI, USA). All stock solutions were prepared in methanol to

Field Code Changed

Field Code Changed

Field Code Changed

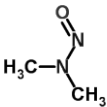
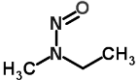
Field Code Changed

Field Code Changed

110 obtain 1 µg/mL of each chemical and were stored at 4 °C in the dark. Both chemicals can be  
 111 classified as hydrophilic and neutral (uncharged) at environmental pH (pH 6 to 8) [39].

Field Code Changed

112 **Table 1** – Structure and properties of the selected *N*-nitrosamines.

Compound	NDMA	NMEA
Structure		
Molecular formula	C <sub>2</sub> H <sub>6</sub> N <sub>2</sub> O	C <sub>3</sub> H <sub>8</sub> N <sub>2</sub> O
Molecular weight [g/mol]	74.05	88.06
Log <i>D</i> at pH8 <sup>a</sup> [-]	0.04	0.4
pKa at pH8 <sup>a</sup> [-]	3.5	3.4
Minimum projection area <sup>a, b</sup> [nm <sup>2</sup> ]	0.20	0.22

Formatted: Font color: Auto

Formatted: Font color: Auto

Formatted: Font color: Auto

Formatted: Font color: Auto

Formatted: Font color: Auto

Formatted: Font color: Auto

Formatted: Font color: Auto

Formatted: Font color: Auto

Formatted: Font color: Auto

113 <sup>a</sup> Chemicalize (<http://www.chemicalize.org>).

114 <sup>b</sup> Minimum projection area is the area of the compound projected with the minimum plane of  
 115 its circular disk, based on the van der Waals radius.

## 116 2.2. Membranes and membrane treatment system

117 Two commercially available RO membranes – namely ESPA2 and ESPAB – and a prototype  
 118 RO membrane were obtained as flat sheet samples from Hydranautics/Nitto (Osaka, Japan).  
 119 The active skin layers of these membranes have similar chemical ingredients although the  
 120 detailed information is proprietary. The ESPA2 membrane has been employed in many potable  
 121 water reuse schemes [14], while the ESPAB membrane is designed for boron removal and has  
 122 been widely used in the second pass of RO seawater desalination plants. In addition, samples  
 123 of the ESPAB and Prototype membranes were also subjected to heat treatment to alter the  
 124 physical properties. These heat-treated samples are designated as heated ESPAB and heated  
 125 Prototype, respectively. Thus, in total, five different membrane samples were used in this  
 126 investigation.

Field Code Changed

## 127 **2.3. Experimental protocols**

### 128 2.3.1. Heat treatment

129 Heat treatment was conducted by heating the RO membrane coupons in 80 °C ultrapure water  
130 solution. The RO membrane coupons were first rinsed with ultrapure water (18.0 MΩcm).  
131 Thereafter, each coupon was stored in a 200 mL beaker filled with ultrapure water, and the  
132 beakers were placed in a temperature-controlled water bath (SWB-11A, AS ONE, Osaka,  
133 Japan) that maintained the water temperature at 80 °C. After 4 h of heat treatment, the  
134 membrane coupons were rinsed with ultrapure water and stored at 4 °C in the dark.

### 135 2.3.2. RO filtration experiments

136 The separation of NDMA and NMEA by each RO membrane was evaluated in ultrapure water  
137 using the bench-scale cross-flow RO system (**Fig. S1**). Filtration experiments were started with  
138 permeance evaluation in which RO membrane filtration experiments were conducted with  
139 ultrapure water at 2000 kPa to measure the pure water permeance. Thereafter, NDMA and  
140 NMEA stock solution was added to obtain 200 ng/L of each compound in the feed solution.  
141 The membrane system was operated at a 20 L/m<sup>2</sup>h permeate flux and 20 °C feed temperature.  
142 Concentrations of NDMA and NMEA were determined by high-performance liquid  
143 chromatography-photochemical reaction-chemiluminescence as described in our previous  
144 studies [40, 41]. The passage is defined as  $R = 100 \times C_p/C_f$ , where  $C_p$  and  $C_f$  are solute  
145 concentration in the permeate and feed, respectively.

## 146 **2.4. Membrane characterisations**

### 147 2.4.1. Surface chemistry

148 Major functional groups of RO membranes was analysed using Fourier transform infrared  
149 spectroscopy (FTIR) spectrophotometer (Nicolet iS5, Thermo Fisher Scientific, Waltham, MA,  
150 USA) in attenuated total reflection (ATR) method. The RO membrane samples were freeze-

Field Code Changed

Formatted: Font color: Auto



151 dried for 24 hours using a freeze drier (FD-1000, Tokyo Rikakikai, Tokyo, Japan). The  
152 spectrum was obtained in the range of 400-4000 cm<sup>-1</sup> at 1 cm<sup>-1</sup> resolution.

#### 153 2.4.2. Positron annihilation lifetime spectroscopy (PALS)

154 The free-volume hole-radius of each RO membrane was measured using PALS with a slow  
155 positron beam that is housed at the National Institute of Advanced Industrial Science and  
156 Technology (AIST) in Tsukuba, Japan. Details of PALS for the analysis of RO membranes are  
157 provided elsewhere [9]. The radius of free-volume hole ( $r$ ) of the skin layer in RO membranes  
158 was determined from the pick-off annihilation lifetime of *ortho*-positronium ( $\tau_{o-Ps}$ ) using the  
159 Tao-Eldrup model [42, 43]:

$$160 \tau_{o-Ps} = 0.5 \left[ 1 - \frac{r}{r+0.166} + \frac{1}{2\pi} \sin\left(\frac{2\pi r}{r+0.166}\right) \right]^{-1} \quad (1)$$

161 where  $r$  ( $< 1$ nm) is approximated as a spherical shape. Positron irradiation was carried out  
162 under vacuum ( $\sim 10^{-5}$  Pa) and about  $2 \times 10^6$  positron annihilation events were collected for the  
163 positron lifetime spectrum of each sample. Spectra were analysed using a non-linear least-  
164 squares fitting program. Unless otherwise stated, the incident energy ( $E_{in}$ ) was set at 1.0 keV,  
165 which corresponds to a mean implantation depth of 31 nm from the top (implantation depth  
166 range = 0–90 nm) with a material density of 1.3 g/cm<sup>3</sup> (**Fig. 1**). This incident energy was  
167 selected according to previous studies [18, 19] that revealed the lowest free-volume hole-radius  
168 of polyamide RO at 1.0 keV. The dry material density of RO membranes (1.3 g/cm<sup>3</sup>) was  
169 determined based on the data reported by Kolev and Freger [44].

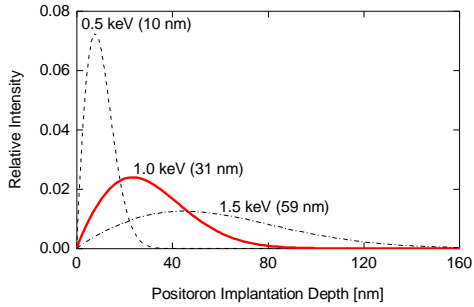
Field Code Changed

Field Code Changed

Field Code Changed

Field Code Changed

Field Code Changed



170

171 **Fig. 1** – Distribution of positron implantation depth in a polyamide membrane sample with a  
 172 material density of 1.3 g/cm<sup>3</sup> at a positron incident energy of 0.5, 1.0 or 1.5 keV. The mean  
 173 implantation depth at each positron incident energy is shown in brackets.

174 2.4.3. Atomic force microscopic analysis

175 Membrane surface area was analysed using an atomic force microscope (AFM) (MFP-3D-SA,  
 176 Asylum Research – Oxford Instruments Company, CA, USA). Membranes underwent sample  
 177 pre-treatment steps involving the replacement of water in the membranes with tert-Butyl  
 178 alcohol followed by freeze drying. Images were obtained in air using tapping mode with a  
 179 silicate cantilever. The scanning area was 5 μm × 5 μm. The effective surface area of each  
 180 membrane was calculated based on the data of three samples. Effective surface area here was  
 181 defined as a ratio between the actual (measured) area and the sample area as described in the  
 182 following formula:

183 
$$\text{Effective surface area [\%]} = \frac{\text{Actual area } [\mu\text{m}^2]}{\text{Sample area } [\mu\text{m}^2]} \times 100 \quad (2)$$

184 2.4.4. Field emission scanning electron microscopic analysis

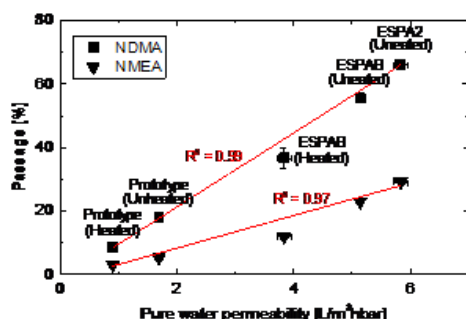
185 Cross-sectional images of the RO membrane skin layer were attained using a field emission -  
 186 scanning electron microscope (FE-SEM) instrument (S-4800, Hitachi, Japan) at 3 kV  
 187 accelerating voltage. Cross-sections of each membrane sample were prepared by freeze-

188 fracturing wet membranes in liquid nitrogen followed by air drying. Thereafter, the target  
189 cross-sectional area was coated with conductive material prior to the analysis. The thickness of  
190 the skin layer of each RO membrane was calculated by determining the average of 5 different  
191 locations.

### 192 **3. Results and discussion**

#### 193 **3.1. Solute permeation**

194 The five RO membrane samples examined in this study spanned over a large range of water  
195 permeance as well as solute passage with respect to both NDMA and NEMA (**Fig. 2**). Heat  
196 treatment was effective to reduce solute passage and water permeance. After heat treatment,  
197 NDMA passage through the ESPAB and the Prototype membranes decreased from 56 to 37%  
198 and from 18 to 9%, respectively. The pure water permeance of these membrane also  
199 proportionally decreased as can be seen from **Fig. 2**. A strong linear correlation between solute  
200 passage with respect to both NDMA and NMEA and water permeance can be confirmed in **Fig.**  
201 **2**. As noted in section 2.2, all five RO membrane samples were from the same manufacturer  
202 with similar chemical ingredients of the active skin layer. Thus, data from **Fig. 2** allow for a  
203 systematic investigation of the role of the active skin layer in transport of small and neutral  
204 solutes as well as water across the membrane.



205

206 **Fig. 2** – Correlation between the passage of NDMA and NMEA in pure water, and pure water  
 207 permeance (feed temperature = 20.0 ± 0.1 °C and permeate flux = 20 L/m²h). Error bars show  
 208 the range of two replicate experiments.

### 209 3.2. Characterisations of the RO skin layer

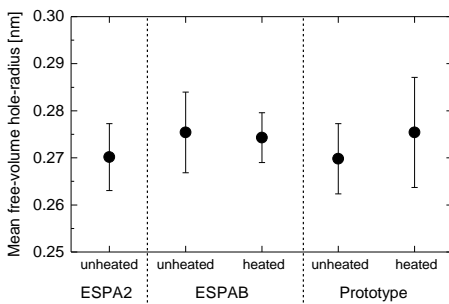
#### 210 3.2.1. Membrane chemistry

211 Variation in the top layer chemistry of RO membranes can be qualitatively evaluated by  
 212 examining the FTIR spectra [45, 46]. Notable peaks for fully aromatic polyamide were  
 213 observed at 1668, 1608 and 1539 cm<sup>-1</sup> that correspond to C=O and C-N stretching and C-C-N  
 214 deformation vibration (amide I), N-H deformation vibration and C=C ring stretching vibration  
 215 of aromatic amide, and N-H in-plane bending and N-C stretching vibration of a -CO-NH- group  
 216 (amide II), respectively [47] (**Fig. S2**). Peaks at 1586, 1505, 1488 and 1245 cm<sup>-1</sup> can be  
 217 assignable to polysulfone. The ratio in peak intensity between 1668 cm<sup>-1</sup> (C=O stretching of  
 218 the amide group formed by the reaction between diamine and acid chloride) and 1245 cm<sup>-1</sup> (C-  
 219 O stretching of the polysulfone support) was 0.21, 0.21 and 0.17 for ESPA2, ESPAB and  
 220 Prototype, respectively. This indicates that these RO membranes have a similar chemical  
 221 ~~property composition~~. ~~In contrast, it is noted that~~ heat treatment increased the peak intensity  
 222 ratio from 0.21 to 0.30 and from 0.17 to 0.18 for ESPAB and Prototype membrane, respectively.  
 223 The cause of the changes in the peak intensity for ESPAB after heat treatment remains unclear,  
 224 but it will be in the scope of our future study.

Formatted: Font color: Auto

225 3.2.2. Free-volume hole-radius

226 The mean free-volume hole-radius of the selected RO membranes was determined at a mean  
227 implantation depth of 31 nm using  $\tau_{o-Ps}$  values (pick-off annihilation lifetime of *o*-Ps) from  
228 PALS analysis (**Table S3**). The free-volume hole-radius of the three unheated RO membranes  
229 (i.e. ESPA2, ESPAB and Prototype) was almost identical, ranging from 0.270 to 0.275 nm (**Fig.**  
230 **3**). Heat treatment did not show any discernible impact on the free-volume hole-radius. It is  
231 noteworthy that PALS analysis at other implantation depths (i.e. 10 and 59 nm) of the ESPAB  
232 membrane did not show any significant variation in the free-volume hole-radius due to heat  
233 treatment (**Fig. S4**). It is noted that current PALS technique cannot confirm a small difference  
234 in free-volume hole-radius of RO membranes less than 0.01 nm due to the inherent errors in  
235 PALS and the inhomogeneity of the membrane samples. Thus, the free-volume hole-radius of  
236 all five membrane samples in **Fig. 3** are considered to be similar.



237 **Fig. 3** – Free-volume hole-radius of the five RO membranes. The data here is the average and  
238 range of two replicates.

240 The cross-sectional areas of spherical free-volume holes with radii of 0.270 and 0.275 nm are  
241 0.23 and 0.24 nm<sup>2</sup>, respectively. These values are comparable to the minimum projection area  
242 of NDMA (0.20 nm<sup>2</sup>) and NMEA (0.22 nm<sup>2</sup>) (**Table 1**). Because the passage of NDMA and  
243 NMEA varied with a difference of only 0.02 nm<sup>2</sup> in the minimum projection area of the two

244 molecules, a variation of 0.01 nm<sup>2</sup> in free-volume hole-area among the five RO membranes  
245 may still be an important factor. However, there was no observable correlation between the  
246 measured free-volume hole-radius and the passage of NDMA and NMEA (**Fig. S5**). Given the  
247 similar free-volume hole-size of the five membrane samples, these results suggest that a factor  
248 other than the free-volume hole-size can also govern the permeation of NDMA and NMEA by  
249 these RO membranes.

### 250 3.2.3. Effective surface area

251 The effective membrane surface area was determined by taking into account the topography of  
252 the RO skin layer at the microscopic level (i.e. surface roughness) using AFM. Indeed, at the  
253 microscopic level, the effective membrane surface area can differ considerably from the surface  
254 area normally used to calculate the permeate flux [9]. It is noted that permeate flux  
255 considerably influences NDMA permeation [13]. Since the skin layer can play an important  
256 role in solute permeation through the RO membrane as proposed in literature [30, 38], it is  
257 important to take into account the effective membrane surface area when assessing solute  
258 permeation.

259 Despite the large variation in the visualized “ridge-and-valley” structure among the three  
260 different types of RO membranes (i.e. ESPA2, ESPAB and Prototype), their effective surface  
261 area was almost identical, ranging from 198 and 212% (**Fig. 4**). In other words, the effective  
262 membrane surface area at the microscopic level is approximately two times the plain area.  
263 Likewise, heat treatment did not cause any discernible changes in the effective surface area.  
264 Results from **Fig. 4** confirm that separation experiments in this study were also at the same  
265 permeate flux for a systematic comparison of solute permeation among all selected RO  
266 membranes. More importantly, the observation of the large variation in permeance (**Fig. 2**) and  
267 almost identical effective surface area (**Fig. 4**) among the RO membranes suggests that in this

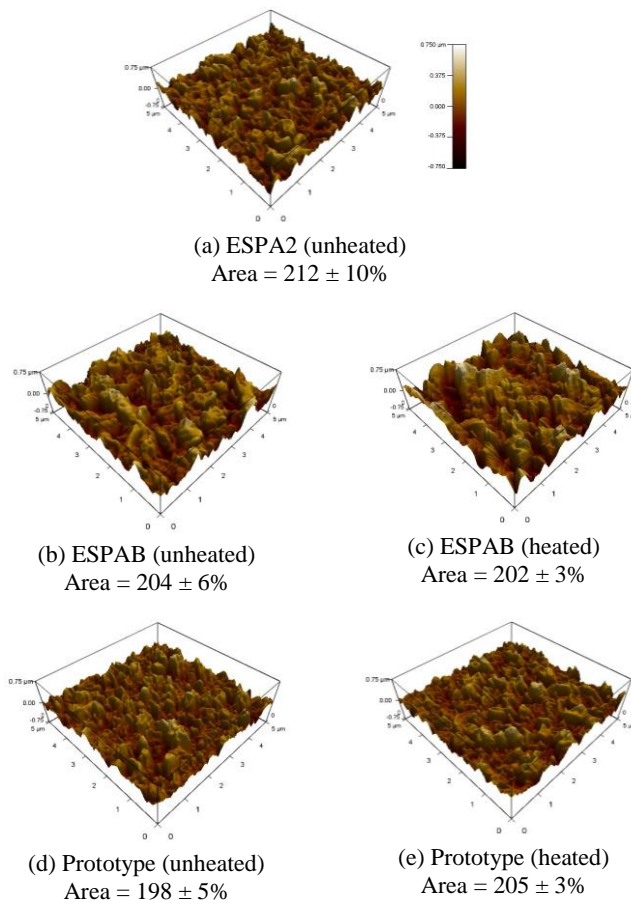
Field Code Changed

Field Code Changed

Field Code Changed

268 study, water permeance is not influenced by the effective surface area of the RO skin layer. It  
 269 is noteworthy that the surface area determined by AFM does not necessarily represent the entire  
 270 surface area. Surface areas through which feed solution can penetrate include the backside of  
 271 bent protuberance and confined rumpled films with packed protuberances that cannot be  
 272 measured by AFM [32]. Therefore, actual surface area taking account of all morphology is  
 273 necessary to conclusively determine the role of surface area for water permeance.

Field Code Changed



274 **Fig. 4** – AFM images of the five RO membranes. The surface area (and error) is determined  
 275 from the average (and measurement variation) of three membrane coupons.

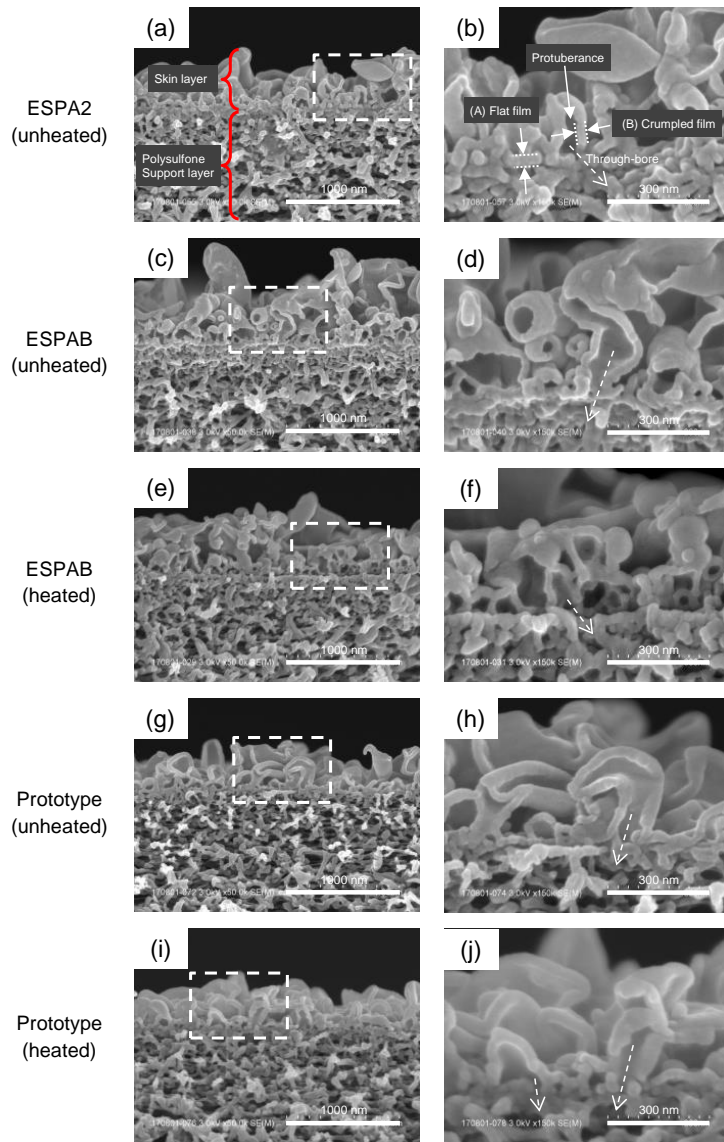
276 3.2.4. Thickness

277 The thickness of the skin layer of the selected RO membranes was evaluated using a cross-  
278 sectional view obtained by FE-SEM. The FE-SEM analysis (**Fig. 5**) revealed a distinctive  
279 “ridge-and-valley” structure and a hollow interior of crumpled nodules throughout the skin  
280 layer of all RO membranes investigated in this study. These complex structures are similar to  
281 other commercial RO membranes recently reported in literature [36-38]. The estimated  
282 thickness of the skin layer was 300-400 nm for ESPA2 and ESPAB RO membranes and 200-  
283 300 nm for Prototype RO membranes. There was no apparent change in the skin layer thickness  
284 after heat treatment. The skin layer of these membranes comprised of two major polyamide  
285 films (A) a flat polyamide film that forms a film base at the interface with the polysulfone  
286 support layer and (B) a crumpled polyamide film that forms crumpled nodules with internal  
287 hollow structure (also called as protuberance) (**Fig. 5**). Ultrahigh resolution FE-SEM images  
288 in **Fig. 5** show a similar thickness between the flat polyamide film and crumpled polyamide  
289 film. In addition, it appears that the crumpled polyamide film is almost always on top of the  
290 flat polyamide film. Using SEM, Yan et al. [37] also reported that the ESPA2 RO membrane  
291 has a through-bore that interconnects the cavity of the protuberance and open structure of the  
292 polysulfone support layer. The interconnections can also be found at the other four RO  
293 membranes used in this study. The majority of the protuberances did not appear to have  
294 interconnections. Although high water permeance of RO membranes (e.g. ESPA2) can be  
295 associated with the number of the interconnections, it was not possible to quantify the  
296 connectivity through the FE-SEM cross-sectional images.

Field Code Changed

Field Code Changed





Formatted: Centered

Formatted: Centered

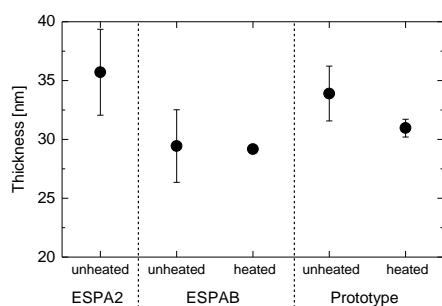
Formatted: Centered

Formatted: Centered

Formatted: Centered

298 **Fig. 5** – FE-SEM cross-sectional images of the five RO membranes: (a, c, e, g, i) skin &  
 299 polysulfone layers (scale = 1000 nm) and (b, d, f, h, j) areas enclosed with dash lines in the  
 300 skin & polysulfone layers (scale = 300 nm).

301 Given the importance of the crumpled polyamide films on water and solute permeation [30,  
302 37], the crumpled film thickness was measured for all the RO membranes. It is noted that the  
303 values were attained through two representative FE-SEM images; thus, there could be a  
304 variation in thickness throughout the RO membranes. The results revealed that unheated  
305 ESPA2, ESPAB and Prototype RO membranes had similar crumpled film thickness of 36, 29,  
306 and 34 nm, respectively (**Fig. 6**). Results in **Fig. 6** indicate that there was no discernible  
307 variation in thickness among the three RO membranes in this study. In addition, heat treatment  
308 did not appear to alter the crumpled film thickness. Indeed, differences in the crumpled film  
309 thickness between heated and unheated samples were within the measurement error margin (i.e.  
310 standard deviation of two samples of the same membrane). As a result, in this study, variation  
311 in water flux and the passage of NDMA and NMEA cannot be attributed to the measured  
312 crumpled film thickness (**Fig. S7**), suggesting that other skin layer properties such as  
313 conformation of the crumpled polyamide films could also govern their permeation.



314

315 **Fig. 6** – Thickness of the crumpled film of the five RO membranes. The thickness was  
316 determined based on two RO membrane coupons, each of which was measured at 5 locations  
317 (**Table S6**).

318 **3.3. Discussions**

319 Comprehensive analysis of the skin layer of five RO membrane samples using PALS, FE-SEM  
320 and AFM revealed that there could be other RO skin layer properties besides the free-volume  
321 hole-radius and thickness of the crumpled film that can govern water and solute permeation.  
322 This is a significant finding in membrane transport, because the free-volume hole-radius and  
323 thickness of the crumpled film have often been considered the only membrane properties  
324 governing the membrane transport.

325 FE-SEM images obtained here identified that the free-volume hole-radius analysed by PALS  
326 was likely to result from the crumpled polyamide film. According to the distribution of positron  
327 implantation depth (**Fig. 1**), most positrons of PALS at a positron incident energy of 1 keV  
328 were expected to have annihilated within the crumpled polyamide films that have the thickness  
329 of about 30 nm. The flat polyamide film is mostly covered by several layers of the crumpled  
330 film and it is 300 to 400 nm away from the top ridge (**Fig. 5**). Thus, the flat polyamide film  
331 located at the interface with the polysulfone supporting layer is not accessible by positrons with  
332 1 keV. Although the flat polyamide film beneath the crumpled films can be reached by  
333 increasing the positron incident energy (**Fig. 1**), increasing the incident energy also broadens  
334 out the positron implantation depth distribution, meaning that signals can be obtained from  
335 both the flat and crumpled films. As a result, thickness of the flat film that has far less surface  
336 area than the crumpled film cannot be accurately determined. If the flat polyamide film plays  
337 an important role in solute permeation, a sample preparation method that enables us to  
338 preferentially analyse the flat polyamide films should be developed.

339 In regard to the flat polyamide film, perhaps water permeance and separation performance of  
340 the selected RO membranes is related to the degree of the interconnections between the cavity  
341 of the protuberance and the open structure of the polysulfone support layer. In other words, RO

342 membranes with less interconnections have less water permeance but high separation capability.

343 The importance of hollow protuberance on the water permeance of RO membranes has been  
344 confirmed by Pacheco et al. [48] who evaluated 3D images of two commercial RO membranes  
345 using TEM tomography technique. The FE-SEM cross-sectional images in Fig. 5 revealed that  
346 not all of the protuberances have interconnections toward the polysulfone support layer.  
347 Protuberances without interconnections allow the solute and solvent (water) to permeate  
348 through two barriers – crumpled film and flat film, which could reduce water permeance but  
349 improve the separation performance. The projected area TEM technique previously reported  
350 by Pacheco et al. [36] and Yan et al. [37] has the potential to visualize the structure inside the  
351 ridges including the interconnections from its top view, but the correlation between the  
352 interconnections and separation performance has not yet been quantified.

353 There are some other limitations and challenges for the characterization of the RO skin layer  
354 with respect to PALS analysis. The analysis here was conducted under dry conditions, while  
355 wet RO membranes may have swelling effects [49], which can expand the polymer network  
356 and alter the water permeance and selectivity [50, 51]. In addition, the size distribution of free-  
357 volume holes may be more important than mean free-volume hole-radius, because the narrower  
358 passages connecting the major free-volume holes could actually determine solute permeations  
359 as suggested by Dražević et al. [52]. More accurate analysis with wet membrane samples and  
360 the determination of size distribution of free-volume holes requires a significant improvement  
361 in PALS method, thus, it is a scope of our future study.

362 In addition to the swelling effects, chemical properties of the internal skin layer could be a  
363 major contributor to a variation in diffusion coefficient and sorption coefficient of water and  
364 solutes, which ultimately leads to a variation in their water permeance and separation  
365 performance. Typically, increases in the degree of polyamide cross-linking can cause less water

Formatted: Font color: Auto

Field Code Changed

Field Code Changed

Field Code Changed

Field Code Changed

Field Code Changed

366 and solutes to sorb onto the polymer due to restriction in swelling effects [53]. This could cause  
367 a decrease in both effective water and salt diffusion coefficients [54], leading to a decrease in  
368 water permeance but an increase in selectivity ( $D_w/D_s$ ) (trade-off theory) [26]. If that is the case,  
369 chemical properties of the skin layer such as cross-linking levels should be more important  
370 than the physical properties analysed in this study (i.e. free-volume hole-radius and thickness)  
371 to determine the major skin layer properties.

#### 372 **4. Conclusions**

373 This study shows that RO membranes with distinct separation performance and water  
374 permeance can have similar crumpled film properties including free-volume hole-size and  
375 thickness. PALS, AFM and FE-SEM revealed that major crumpled polyamide film properties  
376 such as free-volume hole-size, effective surface area and thickness are almost identical among  
377 three different types of unheated RO (ESPA2, ESPAB and Prototype) and two heated RO  
378 (ESPAB and Prototype). The results suggest that there exist at least another RO skin layer  
379 property other than the free-volume hole-size and thickness that can also govern the transport  
380 of water and small and neutral solutes such as NDMA and NMEA that are of significant  
381 concern in potable water reuse. Such property is likely to be the protuberance conformation or  
382 interconnectivity of the protuberance within the membrane polyamide skin layer. In addition,  
383 FE-SEM data also reveal that current PALS technique may not be suitable for determining  
384 free-volume hole-radius of the flat polyamide film located at the interface between the  
385 polyamide skin and the polysulfone supporting layer beneath the crumpled polyamide films.  
386 Further advances in analytical technique that allows for the quantification of interconnections  
387 between the protuberances and the polysulfone support layer, the comprehensive  
388 characterisation of RO membranes by PALS (size distribution and wet conditions), and the

Field Code Changed

Field Code Changed

Field Code Changed

389 evaluation of chemical properties of the polyamide films is necessary to fully decode the  
390 permeation mechanism of NDMA.

## 391 5. Acknowledgements

392 This work was supported by KWEF Research Grant Program; JSPS KAKENHI Grant Number  
393 JP16H06104; and AIST Nanocharacterization Facility (ANCF) platform as a program of  
394 "Nanotechnology Platform" of the Ministry of Education, Culture, Sports, Science and  
395 Technology (MEXT), Japan. We also thank Hydranautics/Nitto for providing RO membrane  
396 samples for this investigation.

## 397 6. References

- 398 [1] US Environmental Protection Agency, Integrated Risk Information System (IRIS), N-  
399 nitrosodimethylamine. Office of Research and Development (ORD), National Center  
400 for Environmental Assessment (1987) [www.epa.gov/iris/subst/0045.htm](http://www.epa.gov/iris/subst/0045.htm), in, 1987.
- 401 [2] M.J. Farré, K. Döderer, L. Hearn, Y. Poussade, J. Keller, W. Gernjak, Understanding  
402 the operational parameters affecting NDMA formation at Advanced Water Treatment  
403 Plants, *J. Hazard. Mater.*, 185 (2011) 1575-1581.
- 404 [3] C. Bellona, J.E. Drewes, G. Oelker, J. Luna, G. Filteau, G. Amy, Comparing  
405 nanofiltration and reverse osmosis for drinking water augmentation, *Journal AWWA*,  
406 100 (2008) 102-116.
- 407 [4] T. Fujioka, S.J. Khan, J.A. McDonald, A. Roux, Y. Poussade, J.E. Drewes, L.D.  
408 Nghiem, *N-nitrosamine rejection by reverse osmosis membranes: A full-scale study*,  
409 *Water Res.*, 47 (2013) 6141-6148.
- 410 [5] M.H. Plumlee, M. López-Mesas, A. Heidlberger, K.P. Ishida, M. Reinhard, N-  
411 nitrosodimethylamine (NDMA) removal by reverse osmosis and UV treatment and  
412 analysis via LC-MS/MS, *Water Res.*, 42 (2008) 347-355.
- 413 [6] CDPH, NDMA and other Nitrosamines - Drinking water issues, California Department  
414 of Public Health 2011.
- 415 [7] NRMCC, EPHC, AHMC, Australian guidelines for water recycling: Managing health  
416 and environmental risks (Phase 2): Augmentation of drinking water supplies,  
417 Environment Protection and Heritage Council, National Health and Medical Research  
418 Council, Natural Resource Management Ministerial Council, Canberra, 2008.
- 419 [8] H.L. Leverenz, G. Tchobanoglous, T. Asano, Direct potable reuse: A future imperative,  
420 *Journal of Water Reuse and Desalination*, 1 (2011) 2-10.

Field Code Changed

- 421 [9] T. Fujioka, N. Oshima, R. Suzuki, W.E. Price, L.D. Nghiem, Probing the internal  
422 structure of reverse osmosis membranes by positron annihilation lifetime spectroscopy:  
423 Gaining more insight into the transport of water and small solutes, *J. Membr. Sci.*, 486  
424 (2015) 106-118.
- 425 [10] A.R.D. Verliefde, S.G.J. Heijman, E.R. Cornelissen, G.L. Amy, B. Van der Bruggen,  
426 J.C. van Dijk, Rejection of trace organic pollutants with high pressure membranes  
427 (NF/RO), *Environ. Prog.*, 27 (2008) 180-188.
- 428 [11] C. Bellona, J.E. Drewes, P. Xu, G. Amy, Factors affecting the rejection of organic  
429 solutes during NF/RO treatment - A literature review, *Water Res.*, 38 (2004) 2795-2809.
- 430 [12] L.D. Nghiem, P.J. Coleman, NF/RO filtration of the hydrophobic ionogenic compound  
431 triclosan: Transport mechanisms and the influence of membrane fouling, *Sep. Purif.*  
432 *Technol.*, 62 (2008) 709-716.
- 433 [13] T. Fujioka, L.D. Nghiem, S.J. Khan, J.A. McDonald, Y. Poussade, J.E. Drewes, Effects  
434 of feed solution characteristics on the rejection of *N*-nitrosamines by reverse osmosis  
435 membranes, *J. Membr. Sci.*, 409-410 (2012) 66-74.
- 436 [14] T. Fujioka, S.J. Khan, Y. Poussade, J.E. Drewes, L.D. Nghiem, *N*-nitrosamine removal  
437 by reverse osmosis for indirect potable water reuse – A critical review based on  
438 observations from laboratory-, pilot- and full-scale studies, *Sep. Purif. Technol.*, 98  
439 (2012) 503-515.
- 440 [15] Y. Kiso, K. Muroshige, T. Oguchi, M. Hirose, T. Ohara, T. Shintani, Pore radius  
441 estimation based on organic solute molecular shape and effects of pressure on pore  
442 radius for a reverse osmosis membrane, *J. Membr. Sci.*, 369 (2011) 290-298.
- 443 [16] S.H. Kim, S.-Y. Kwak, T. Suzuki, Positron annihilation spectroscopic evidence to  
444 demonstrate the flux-enhancement mechanism in morphology-controlled thin-film-  
445 composite (TFC) membrane, *Environ. Sci. Technol.*, 39 (2005) 1764-1770.
- 446 [17] T. Fujioka, N. Oshima, R. Suzuki, S.J. Khan, A. Roux, Y. Poussade, J.E. Drewes, L.D.  
447 Nghiem, Rejection of small and uncharged chemicals of emerging concern by reverse  
448 osmosis membranes: The role of free volume space within the active skin layer, *Sep.*  
449 *Purif. Technol.*, 116 (2013) 426-432.
- 450 [18] Z. Chen, K. Ito, H. Yanagishita, N. Oshima, R. Suzuki, Y. Kobayashi, Correlation study  
451 between free-volume holes and molecular separations of composite membranes for  
452 reverse osmosis processes by means of variable-energy positron annihilation  
453 techniques, *J. Phys. Chem. C*, 115 (2011) 18055-18060.
- 454 [19] K. Ito, Z. Chen, W. Zhou, N. Oshima, H. Yanagishita, R. Suzuki, Y. Kobayashi,  
455 Subnanoscopic holes in composite membranes for desalination elucidated by energy-  
456 tunable positron annihilation, *Jpn. J. Poly. Sci. Technol.*, 69 (2012) 443-447.
- 457 [20] M. Henmi, Y. Fusaoka, H. Tomioka, M. Kurihara, High performance RO membranes  
458 for desalination and wastewater reclamation and their operation results, *Water Sci.*  
459 *Technol.*, 62 (2010) 2134-2140.

- 460 [21] T. Sasaki, H. Tomioka, K. Nakatsuji, Composite semipermeable membrane, production  
461 process thereof, and element, fluid separation equipment and treatment method for  
462 boron-containing water using the same, in: U.S. Patent (Ed.) United States Patent,  
463 Toray Industries, Inc., USA, 2010.
- 464 [22] T. Fujioka, N. Oshima, R. Suzuki, M. Higgins, W.E. Price, R.K. Henderson, L.D.  
465 Nghiem, Effect of heat treatment on fouling resistance and the rejection of small and  
466 neutral solutes by reverse osmosis membranes, *Water Sci. Technol. Water Supply*, 15  
467 (2015) 510-516.
- 468 [23] J.G. Wijmans, R.W. Baker, The solution-diffusion model: a review, *J. Membr. Sci.*,  
469 107 (1995) 1-21.
- 470 [24] S. Bandini, L. Bruni, 2.04 - Transport Phenomena in Nanofiltration Membranes, in: E.  
471 Drioli, L. Giorno (Eds.) *Comprehensive Membrane Science and Engineering*, Elsevier,  
472 Oxford, 2010, pp. 67-89.
- 473 [25] J. Wang, D.S. Dlamini, A.K. Mishra, M.T.M. Pendergast, M.C.Y. Wong, B.B. Mamba,  
474 V. Freger, A.R.D. Verliefe, E.M.V. Hoek, A critical review of transport through  
475 osmotic membranes, *J. Membr. Sci.*, 454 (2014) 516-537.
- 476 [26] G.M. Geise, H.B. Park, A.C. Sagle, B.D. Freeman, J.E. McGrath, Water permeability  
477 and water/salt selectivity tradeoff in polymers for desalination, *J. Membr. Sci.*, 369  
478 (2011) 130-138.
- 479 [27] H. Ju, A.C. Sagle, B.D. Freeman, J.I. Mardel, A.J. Hill, Characterization of sodium  
480 chloride and water transport in crosslinked poly(ethylene oxide) hydrogels, *J. Membr.*  
481 *Sci.*, 358 (2010) 131-141.
- 482 [28] M. Hirose, H. Ito, Y. Kamiyama, Effect of skin layer surface structures on the flux  
483 behaviour of RO membranes, *J. Membr. Sci.*, 121 (1996) 209-215.
- 484 [29] J.R. Werber, C.O. Osuji, M. Elimelech, Materials for next-generation desalination and  
485 water purification membranes, *Nature Reviews: Materials*, 1 (2016) 16018.
- 486 [30] S. Karan, Z. Jiang, A.G. Livingston, Sub-10 nm polyamide nanofilms with ultrafast  
487 solvent transport for molecular separation, *Science*, 348 (2015) 1347-1351.
- 488 [31] L. Lin, R. Lopez, G.Z. Ramon, O. Coronell, Investigating the void structure of the  
489 polyamide active layers of thin-film composite membranes, *J. Membr. Sci.*, 497 (2016)  
490 365-376.
- 491 [32] M.M. Kłosowski, C.M. McGilvery, Y. Li, P. Abellan, Q. Ramasse, J.T. Cabral, A.G.  
492 Livingston, A.E. Porter, Micro-to nano-scale characterisation of polyamide structures  
493 of the SW30HR RO membrane using advanced electron microscopy and stain tracers,  
494 *J. Membr. Sci.*, 520 (2016) 465-476.
- 495 [33] A.K. Ghosh, B.-H. Jeong, X. Huang, E.M.V. Hoek, Impacts of reaction and curing  
496 conditions on polyamide composite reverse osmosis membrane properties, *J. Membr.*  
497 *Sci.*, 311 (2008) 34-45.



- 498 [34] C.Y. Tang, Y.-N. Kwon, J.O. Leckie, Characterization of humic acid fouled reverse  
499 osmosis and nanofiltration membranes by transmission electron microscopy and  
500 streaming potential measurements, *Environ. Sci. Technol.*, 41 (2006) 942-949.
- 501 [35] V. Freger, Swelling and morphology of the skin layer of polyamide composite  
502 membranes: an atomic force microscopy study, *Environ. Sci. Technol.*, 38 (2004) 3168-  
503 3175.
- 504 [36] F.A. Pacheco, I. Pinnau, M. Reinhard, J.O. Leckie, Characterization of isolated  
505 polyamide thin films of RO and NF membranes using novel TEM techniques, *J. Membr.  
506 Sci.*, 358 (2010) 51-59.
- 507 [37] H. Yan, X. Miao, J. Xu, G. Pan, Y. Zhang, Y. Shi, M. Guo, Y. Liu, The porous structure  
508 of the fully-aromatic polyamide film in reverse osmosis membranes, *J. Membr. Sci.*,  
509 475 (2015) 504-510.
- 510 [38] Y. Li, M.M. Kłosowski, C.M. McGilvery, A.E. Porter, A.G. Livingston, J.T. Cabral,  
511 Probing flow activity in polyamide layer of reverse osmosis membrane with  
512 nanoparticle tracers, *J. Membr. Sci.*, 534 (2017) 9-17.
- 513 [39] B. Van der Bruggen, A. Verliefde, L. Braeken, E.R. Cornelissen, K. Moons, J.Q.J.C.  
514 Verberk, H.J.C. van Dijk, G. Amy, Assessment of a semi-quantitative method for  
515 estimation of the rejection of organic compounds in aqueous solution in nanofiltration,  
516 *J. Chem. Technol. Biotechnol.*, 81 (2006) 1166-1176.
- 517 [40] T. Fujioka, H. Takeuchi, H. Tanaka, L.D. Nghiem, K.P. Ishida, H. Kodamatani, A rapid  
518 and reliable technique for *N*-nitrosodimethylamine analysis in reclaimed water by  
519 HPLC-photochemical reaction-chemiluminescence, *Chemosphere*, 161 (2016) 104-  
520 111.
- 521 [41] H. Kodamatani, H. Yamasaki, T. Sakaguchi, S. Itoh, Y. Iwaya, M. Saga, K. Saito, R.  
522 Kanzaki, T. Tomiyasu, Rapid method for monitoring *N*-nitrosodimethylamine in  
523 drinking water at the ng/L level without pre-concentration using high-performance  
524 liquid chromatography-chemiluminescence detection, *J. Chromatogr. A*, 1460 (2016)  
525 202-206.
- 526 [42] M. Eldrup, D. Lightbody, J.N. Sherwood, The temperature dependence of positron  
527 lifetimes in solid pivalic acid, *Chem. Phys.*, 63 (1981) 51-58.
- 528 [43] S.J. Tao, Positronium annihilation in molecular substances, *J. Chem. Phys.*, 56 (1972)  
529 5499-5510.
- 530 [44] V. Kolev, V. Freger, Hydration, porosity and water dynamics in the polyamide layer  
531 of reverse osmosis membranes: A molecular dynamics study, *Polymer*, 55 (2014) 1420-  
532 1426.
- 533 [45] M. Bass, V. Freger, Facile evaluation of coating thickness on membranes using ATR-  
534 FTIR, *J. Membr. Sci.*, 492 (2015) 348-354.
- 535 [46] E. Dražević, K. Košutić, V. Freger, Permeability and selectivity of reverse osmosis  
536 membranes: Correlation to swelling revisited, *Water Res.*, 49 (2014) 444-452.

- 537 [47] C.Y. Tang, Y.-N. Kwon, J.O. Leckie, Effect of membrane chemistry and coating layer  
538 on physiochemical properties of thin film composite polyamide RO and NF  
539 membranes: I. FTIR and XPS characterization of polyamide and coating layer  
540 chemistry, *Desalination*, 242 (2009) 149-167.
- 541 [48] F. Pacheco, R. Sougrat, M. Reinhard, J.O. Leckie, I. Pinnau, 3D visualization of the  
542 internal nanostructure of polyamide thin films in RO membranes, *J. Membr. Sci.*, 501  
543 (2016) 33-44.
- 544 [49] J. Lee, C.M. Doherty, A.J. Hill, S.E. Kentish, Water vapor sorption and free volume in  
545 the aromatic polyamide layer of reverse osmosis membranes, *J. Membr. Sci.*, 425–426  
546 (2013) 217-226.
- 547 [50] E.P. Chan, A.P. Young, J.-H. Lee, J.Y. Chung, C.M. Stafford, Swelling of ultrathin  
548 crosslinked polyamide water desalination membranes, *J. Polym. Sci., Part B: Polym.*  
549 *Phys.*, 51 (2013) 385-391.
- 550 [51] Y.-H. Huang, W.-C. Chao, W.-S. Hung, Q.-F. An, K.-S. Chang, S.-H. Huang, K.-L.  
551 Tung, K.-R. Lee, J.-Y. Lai, Investigation of fine-structure of polyamide thin-film  
552 composite membrane under swelling effect by positron annihilation lifetime  
553 spectroscopy and molecular dynamics simulation, *J. Membr. Sci.*, 417–418 (2012) 201-  
554 209.
- 555 [52] E. Dražević, K. Košutić, V. Kolev, V. Freger, Does Hindered Transport Theory Apply  
556 to Desalination Membranes?, *Environ. Sci. Technol.*, 48 (2014) 11471-11478.
- 557 [53] G.M. Geise, D.R. Paul, B.D. Freeman, Fundamental water and salt transport properties  
558 of polymeric materials, *Prog. Polym. Sci.*, 39 (2014) 1-42.
- 559 [54] T.A. Jadwin, A.S. Hoffman, W.R. Vieth, Crosslinked poly(hydroxyethyl methacrylate)  
560 membranes for desalination by reverse osmosis, *J. Appl. Polym. Sci.*, 14 (1970) 1339-  
561 1359.
- 562